LABORATORI NAZIONALI DI FRASCATI
SIS-Pubblicazioni

LNF-02/02(P)
10 Aprile 2002

The Trigger System of the KLOE Experiment.

The KLOE Collaboration*

Abstract

We present the design of the trigger system for the KLOE experiment at the Frascati ϕ-factory DAΦNE. The detector consists of a large-volume drift chamber and a calorimeter both immersed in a 0.52 T solenoidal field. The trigger, structured with a first- and a second-decision level, is based on the multiplicity of energy deposits in the calorimeter and of hits in the drift chamber. The selection criteria are described and the efficiency for detecting ϕ decays is evaluated using data.

PACS:29.40.-n

Submitted to Elsevier Science for publication on Nuclear Instruments and Methods A.

* The KLOE Collaboration

M. Adinolfi[j], F. Ambrosino[f], M. Antonelli[b], C. Bini[h], V. Bocci[h], F. Bossi[b], P. Branchini[k,†], G. Cabibbo[h], R. Caloi[h], M. Casarsa[l], G. Cataldi[d,‡], P. Ciambrone[b], E. De Lucia[h], G. De Robertis[a], P. De Simone[b], S. Dell'Agnello[b], A. Denig[b,‡], A. Di Domenico[h], C. Di Donato[f], S. Di Falco[g], A. Doria[f], G. Felici[b], A. Ferrari[k], G. Finocchiaro[b], C. Forti[b], P. Franzini[h], C. Gatti[g], P. Gauzzi[h], E. Gero[b], S. Giovannella[b], E. Graziani[k,†], P. Guarnaccia[a], M. Incagli[g], C. Kuo[c], G. Lanfranchi[b], M. Martemianov[e,b], W. Mei[b], R. Messi[j], M. Moulson[b], S. Müller[c], F. Murtas[b], L. Pacciani[j], M. Palutan[j], E. Pasqualucci[h], L. Passalacqua[b], A. Passeri[k,†], V. Patera[i,b], D. Picca[h], G. Pirozzi[f], L. Pontecorvo[h], M. Primavera[d], F. Ruggieri[a], P. Santangelo[b], E. Santovetti[j], G. Saracino[f], C. Schwick[b,§], B. Sciascia[h], A. Sciubba[i,b], I. Sfiligoi[b], T. Spadaro[h], E. Spiriti[k,†], P. Valente[b], B. Valeriani[c], G. Venanzoni[g], A. Ventura[d]

[a] *Dipartimento di Fisica dell'Università e Sezione INFN, Bari, Italy*
[b] *Laboratori Nazionali di Frascati dell'INFN, Frascati, Italy*
[c] *Institut für Experimentelle Kernphysik, Universität Karlsruhe, Germany*
[d] *Dipartimento di Fisica dell'Università e Sezione INFN, Lecce, Italy*
[e] *Permanent address: Institute for Theoretical and Experimental Physics, Moscow, Russia*
[f] *Dipartimento di Scienze Fisiche dell'Università "Federico II" e Sezione INFN, Napoli, Italy*
[g] *Dipartimento di Fisica dell'Università e Sezione INFN, Pisa, Italy*
[h] *Dipartimento di Fisica dell'Università "La Sapienza" e Sezione INFN, Roma, Italy*
[i] *Dipartimento di Energetica dell'Università "La Sapienza", Roma, Italy*
[j] *Dipartimento di Fisica dell'Università "Tor Vergata" e Sezione INFN, Roma, Italy*
[k] *Dipartimento di Fisica dell'Università "Roma Tre" e Sezione INFN, Roma, Italy*
[l] *Dipartimento di Fisica dell'Università e Sezione INFN, Trieste, Italy*
† *formerly Istituto Superiore di Sanità e Sezione INFN, ISS, Roma, Italy*
‡ *formerly Institut für Experimentelle Kernphysik, Universität Karlsruhe, Germany*
§ *Present address: CERN, Geneva Switzerland*

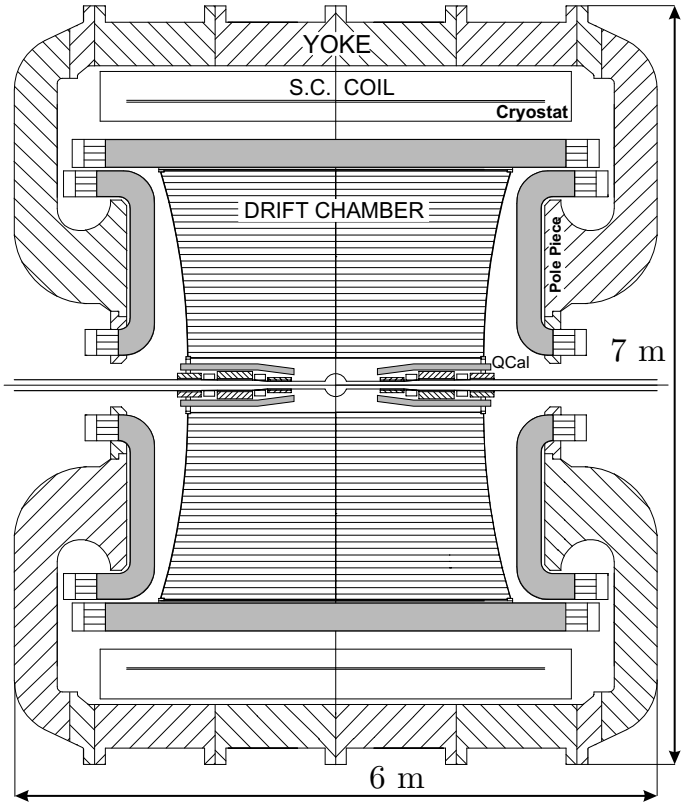

Figure 1: Vertical cross section of the KLOE detector.

1 Introduction

The aim of the KLOE experiment is the study of CPsymmetry violation in K_L decays, and in particular, the measurement of $\Re(\epsilon'/\epsilon)$ to an accuracy of $\sim 1 \times 10^{-4}$ [1][2]. KLOE operates at DAΦNE, the Frascati ϕ–factory, an e^+e^- collider designed to deliver a luminosity of at least 5000 pb^{-1}y^{-1} at the ϕ peak, $E \sim 1020$ MeV. Collisions were first observed in 1999. The maximum DAΦNE luminosity is still below design by about a factor of ten. ϕ-mesons decay to K_S, K_L pairs $\sim$34% of the time. The basic requirement for the trigger is that its efficiency ϵ_T be identical for the $\pi^+\pi^-$ and $\pi^0\pi^0$decays of the K_S and K_L. Ideally, one would like a trigger with $1 - \epsilon_T \ll 1$.

The detector, fig. 1, consists of two elements. Tracking is by means of a drift chamber (DC, [3]), 3.3 m in length and 2 m in radius, with 12582 drift cells organized in 58 concentric stereo layers. The hermetic lead-scintillating fiber electromagnetic calorimeter (EMC, [4]) is divided into a barrel and two endcaps. The barrel is composed of 24 modules, 4.4 m long. Each endcap contains 36 modules of different lengths, which run vertically in a plane perpendicular to the beam axis. Each module is segmented with a granularity of 4.4 $\times$ 4.4 cm^2, five layers in depth, and read-out at each end with photo-

multipliers, forming a column approximately pointing to the interaction region. The total number of calorimeter columns is 488, read out by 4880 tubes. A superconducting coil, surrounding the entire detector, provides a field of 0.52 T.

The signal from each calorimeter tube is processed by an ADC and a TDC. The ADC's operate asynchronously while the TDC's operate in common start. The stop signals from the phototubes are electronically delayed by 200 ns. Drift times are measured by 12,600 digital TDC's running at 1 GHz, operated in common stop mode.

Two triplets of low-β quadrupoles are located between the vacuum pipe and the drift chamber on the two sides of the interaction point. They are surrounded by two compact tile calorimeters (QCAL), with the purpose of increasing the hermeticity of KLOE to photons produced in K_L decays.

Event rates at DAΦNE are high; at the maximum design luminosity of 5×10^{32}cm^{-2}s^{-1} up to 1500 ϕ/s and up to 30,000 Bhabha/s are within KLOE acceptance. We wish to retain all ϕ decays, and for detector calibration, all Bhabha and $\gamma\gamma$ events at large angle, and an appropriate fraction of such events at small angles. The same applies to cosmic-ray particles which enter the detector with a rate of $\sim$3000 Hz. Finally, the trigger must have efficient background rejection in order not to overload the data acquisition system (DAQ, [5]). A maximum event rate of $\sim$10 kHz can be accepted. This last point has turned out to be a major problem in DAΦNE. For reasons which are most likely connected, the luminosity is lower than initially estimated, and background levels are much higher. The trigger system must perform the following basic functions:

1. Produce a trigger for all ϕ events.
2. Recognize Bhabha events and accept a downscaled sample at small angle.
3. Recognize cosmic-ray events and pass a downscaled sample.
4. Reject background.

In addition the trigger must be formed in as short a time as possible and be precisely correlated to the collision time, which is discretized to within $\sim$2.7 ns, the spacing between bunches in DAΦNE.

There are two sources of background. One is Bhabha scattering, which diverges at small angle. Scattered electrons and positrons mostly shower on the low-β quadrupoles inside KLOE. The main background is due to the extremely high particle losses from the DAΦNE beams, which ultimately result in very high photon and electron fluxes in the interaction region.

A general overview of the trigger system architecture is presented in section 2 (for details see ref. [6]). A complete description of all trigger hardware components follows (section 3). The next section is devoted to the description of the trigger operation during two periods of data taking, in late 1999 and in 2000. In the last section, we present results on the trigger efficiency.

2 Overview of the Trigger system

2.1 Introduction

Most ϕ events result in a total energy deposit in the EMC which is a small fraction of the ϕ mass. The same is true for Bhabha events degraded in the low-β quads. The EMC energy spectrum for events tagged by a $K_S \to \pi^+\pi^-$ decay in a run with a luminosity of a few times 10^{31} cm^{-2}s^{-1} is shown in fig. 2. In the same run, a very high rate of events with some energy deposited in the endcaps due to particles lost by the beams is observed. For $E > 100$ MeV, this contribution amounts to about 100 kHz. Machine background also gives single tracks originating from elements of the low-β insertion, some of which have been identified as protons and pions photoproduced in the interaction region. This background gives a rate of $\sim$3 kHz, which is still $\sim$20 times the ϕ rate at this luminosity. The two background classes are also shown in the figure.

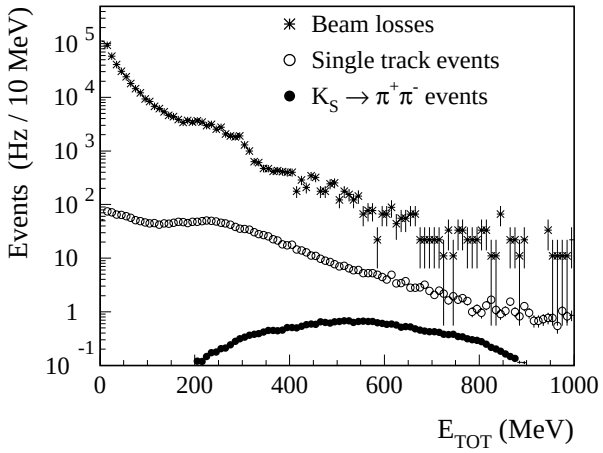

Figure 2: Energy deposited in the EMC by $K_S \to \pi^+\pi^-$ and background events.

Since ϕdecay events have relatively high multiplicity, the EMC trigger is based on the multiplicity of energy deposits above a low threshold, about 50 MeV. Events in which $\phi \to K^0\overline{K}^0$and in which both kaons decay into charged particles have low multiplicity in the calorimeter but give a larger number of hit wires in the DC than do background events. The trigger employs this information as well. The DC trigger greatly improves

the efficiency for $K^{\pm}$ events. The use of both detector elements provides redundancy, which is particularly useful for determining the trigger efficiency.

2.2 General architecture

The 2440 calorimeter elements are combined into 88 groups for trigger purposes. 80 additional overlapping groups guarantee full coverage. Since both ends of the calorimeter modules are read out, the EMC trigger operates on 336 signals. The DC wire count is also obtained by groups, layers and superlayers. The trigger is generated by comparing EMC cluster energies and DC wire counts to programmable thresholds. We have chosen a two level scheme. A first level trigger, T1, is produced with minimal delay and is synchronized with the DAΦNE master clock. A second level trigger, T2, using more information but with less stringent time requirements, is used for readout initialization or T1 abort. The principle is illustrated in fig. 3. Two different thresholds are used for each EMC signal.

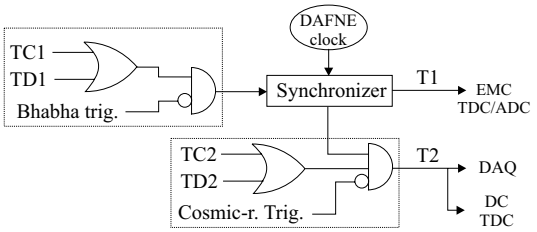

Figure 3: Diagram of the two-level trigger logic.

A low threshold, $\sim$50 MeV, is used to identify ϕ decays (low energy trigger, LET) while a higher threshold at $\sim$350 MeV identifies Bhabha events (Bhabha trigger, BBT). The first and second level EMC trigger signals (TC1 and TC2) are based of the number and locations of the LET signals. The fast DC trigger, TD1, requires $\sim$15 wires in a time window of 250 ns. The second level trigger, TD2, is produced by a count of $\sim$100 wires, accumulated over an interval of $\sim 1\mu$s.

The first level trigger is defined as T1=(TC1 $\oplus$ TD1) $\odot$ NOT(BBT) [1]. Generation of additional T1 signals is vetoed for 2.6 μs, covering the conversion time of all ADC's and TDC's in the system. This leads to an unbiased loss in luminosity of $\sim$1.3%, for a typical T1 rate of 5 kHz. The second level trigger, T2=(TC2 $\oplus$ TD2) $\odot$ T1 $\odot$ NOT(CR), validates T1 and vetoes cosmic rays using the cosmic-ray trigger CR, obtained from the outermost layers of the calorimeter. If no T2 signal is present before the end of the 2.6 μs dead time, all readout is reset.

The trigger signals T1 and T2 have no fixed relation to the bunch crossing time, because of both slewing and time of flight differences from event to event. T1 is syn-

[1] We use the symbols $\odot$, $\oplus$ and NOT for logic and, or and negation respectively.

chronized to the accelerating radio frequency divided by 4, T=10.8 ns, i.e. up to 4 bunch crossing intervals, with a resolution better than 50 ps. The bunch crossing that originated the event is found after event reconstruction.

3 Generation of the trigger

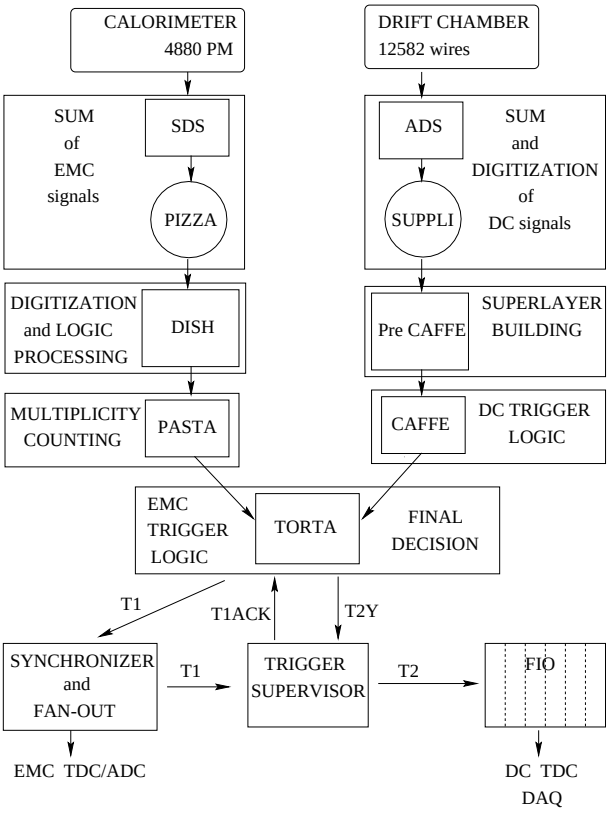

Figure 4: Block diagram of the trigger.

A block diagram of the KLOE trigger is shown in fig. 4.

3.1 The calorimeter trigger circuitry

Calorimeter signals are first processed in analog form, in order to produce local sums of adjacent readout elements with minimal delay. The output signals then become logic signals of appropriate duration by comparison with various thresholds. Finally, combinatorial logic produces the various kinds of triggers.

3.1.1 Summing the EMC signals: SDS and PIZZA boards

The 4880 EMC signals (from both sides of each EMC module) are collected in 164 SDS boards, where five adjacent PM signals, corresponding to one calorimeter column, are added in analog. Signals from 6 adjacent columns, which form a trigger sector, are added together in the PIZZA boards. 48×2 trigger-sector signals are generated for the barrel, corresponding to two overlapping sets of columns (*normal* and *overlap*) as shown in fig. 5. The geometry of the endcaps is more complex. Moreover, more particles are present at

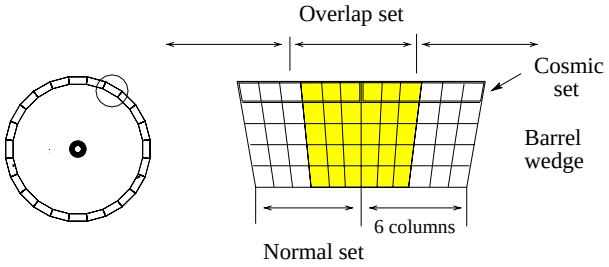

Figure 5: Barrel trigger sectors.

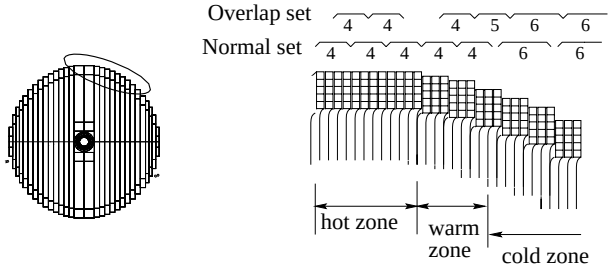

Figure 6: End-cap trigger sectors.

small angle, mostly from background. Each endcap is divided into 20 normal plus 16 overlapping trigger sectors. Sectors cover 4 adjacent columns close to the beam and 5 or 6 elsewhere, see fig. 6. The outer layer of the entire calorimeter is used as a cosmic ray detector. Signals from six adjacent readout elements of the outermost layer are added, for a total of 48 sums in the barrel and 12 sums for each endcap. Six PIZZA boards, two for the barrel and two for each endcap, produce the sector signals. The design of the boards and of the adders is optimized in order to minimize delays and delay differences throughout.

3.1.2 DISH modules

The analog signals from both sides of each calorimeter sector are compared to a high (*hi*) and a low (*lo*) threshold. All thresholds are set by downloading appropriate files to the

trigger system. Thresholds can thus be modified as necessary. Whenever a signal crosses threshold, a logic signal of 35 ns duration, T, is generated. For each sector, sides are labelled A and B in the following. The four logic signals T_A^{lo}, T_A^{hi}, T_B^{lo} and T_B^{hi} generate the **T** signals for each sector according to the logic:

$$\mathbf{T} = \left(\mathrm{T_A^{lo}} \odot \mathrm{T_B^{lo}} \right) \odot \left(\mathrm{T_A^{hi}} \oplus \mathrm{T_B^{hi}} \right) \tag{1}$$

We will show in section 4 how the use of the **T** signals allows the adjustment of the effective threshold along the length of the sectors. The same scheme is used, with appropriate thresholds, for both the LET and BBT triggers, requiring a total of 8 comparators and thresholds per trigger sector. Use of wired-or NAND gates with ECL circuitry minimizes propagation times. The **T** signals are 70 ns long, to cover the spread in particle arrival times. A count of the LET and BBT **T** signals for groups of 6 sectors, N, is also produced. It consists of a signal of amplitude $A = N \times 200$ mV. The status of all comparators above is recorded for all triggers, to allow system monitoring, and is latched at the arrival of the T1 signal. The functional diagram of the DISH (DIgitizer SHaper) board is shown in fig. 7. Two FPGA's provide an interface to the readout system. 30 DISH boards are used

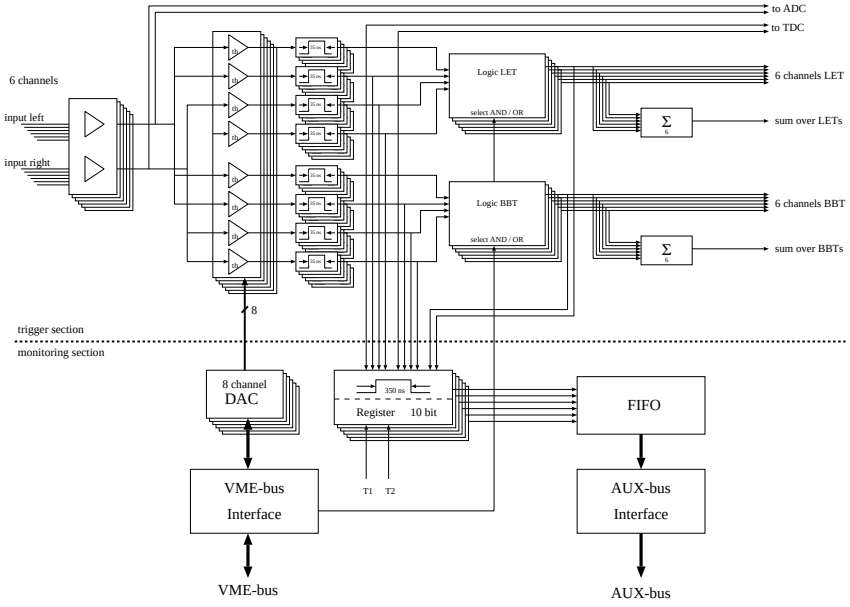

Figure 7: Block diagram of the DISH board.

for the LET and BBT triggers, and 12 are needed for the cosmic-ray trigger, for which only the LET section is used.

3.1.3 Multiplicity counting: the PASTA board

The final sector counting is performed by two PASTA (Precise Analog STAge) boards, one for the barrel and the other for both endcaps. Information from the overlapping sector sets is merged to find the number of LET and BBT local energy deposits. The final multiplicities are obtained by their analog sums, with double counting avoided. The identified cosmic-ray energy deposits are also counted. The input/output delay of the boards is < 20 ns. The PASTA outputs multiplicities of up to three for the LET trigger and up to two for the BBT and cosmic-ray triggers, separately for the barrel and for each endcap. They are listed in table 1. A fraction of the Bhabha scattering events are retained for cali-

	Barrel	Endcap E	Endcap W	N
LET	B1M	E1M	W1M	1
	B2M	E2M	W2M	2
	B3M	E3M	W3M	3
BBT	B1MB	E1MB	W1MB	1
	B2MB	E2MB	W2MB	2
CR	B1CR	E1CR	W1CR	1
	B2CR			2

Table 1: Output signals and multiplicities N from the PASTA board.

bration. Because of the strong increase of the cross section at small angles, it is necessary to appropriately downscale the Bhabha trigger. The BBT signals from the endcap sectors are ORed as shown in fig. 6: appropriate combinations of the signals from the three endcap zones ("hot," "warm," and "cold"), downscaled by the inverse of the relative rates, trigger the acquisition of the event.

All of the output PASTA signals are shaped to a width of 70 ns and then processed by the final trigger generation stage, as explained below.

3.2 The DC trigger hardware

The DC trigger is based on the multiplicity of hit wires, i.e. on the sum of all signals from the 12582 DC sense wires. Since typical threshold values on this sum are very low, especially at the first level, electronic noise is a relevant issue. In order to minimize the effect of coherent noise and differential non-linearities, the sum is performed in three steps (see fig. 8). At each step, signals are summed in analog and digitized at output.

3.2.1 First sums: the ADS and SUPPLI boards

Signals from all DC wire preamplifiers are brought to 272 48-channel ADS (Amplifier/Discriminator/Shaper) boards. On the ADS, each signal is discriminated, buffered,

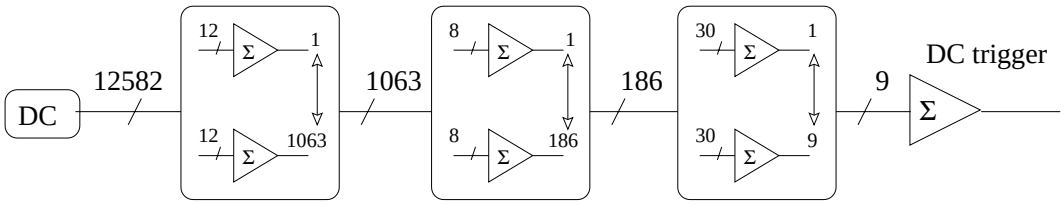

Figure 8: Three level DC hit counting. Note that not all sums are complete.

and split into two different paths. The first path is directed to the DC front-end; the second path is used for the trigger. In the trigger path, signals are shaped at 250 ns. The signals from 12 contiguous wires are summed together, producing a 2 mA/fired-wire current signal. The ADS's in a crate send up to 64 current signals to a SUPPLI (Sum Unit Providing Plane Information) board in the same crate. This module provides analog sums of its input signals, such that the current of each of its outputs is proportional to the number of hit wires in a segment of a given plane of the DC.

3.2.2 Superlayers and formation of logic signals: the pre-CAFFE and CAFFE boards

Multiplicities coded by the SUPPLI output signals are first summed plane-wise on three pre-CAFFE boards; in a second step, on the same boards, they are organized into nine superlayer signals, which represent the multiplicity of hit wires in 4, 6, or 8 contiguous planes. The superlayers map concentric regions of the DC, as shown in fig. 9. They are

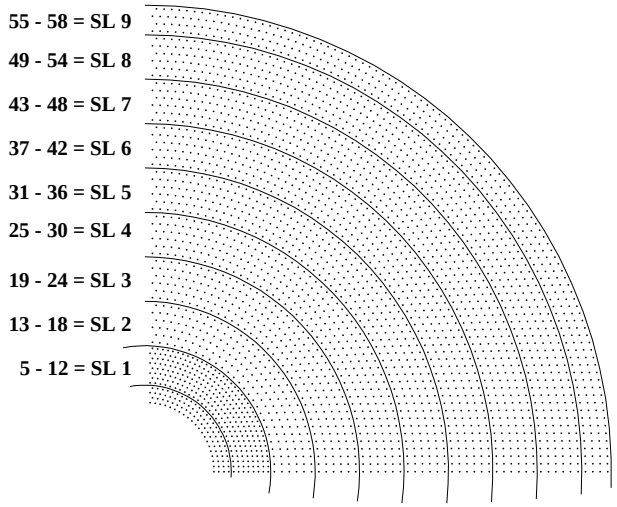

Figure 9: The DC superlayers.

defined to reduce the effect of low-momentum electrons spiralling inside the DC volume, which produce a large number of hit wires in a small region of the chamber. A detailed Monte Carlo simulation has shown that the importance of such events is strongly reduced

by clipping the superlayer signal to a relatively small value (5, typically), while the efficiency on physics signals is not affected [6]. The clipping procedure is applied at a remotely controlled level by the CAFFE (Chamber Activity Fast FEtch) board, which is housed in the same crate as the pre-CAFFE's (see fig. 10). Hereafter, the multiplicity

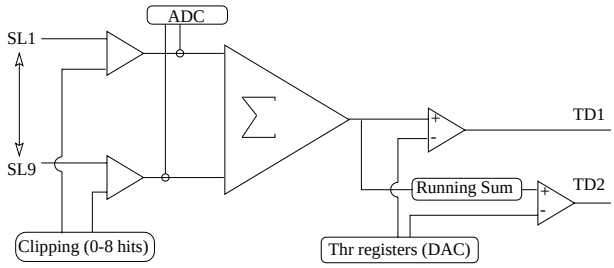

Figure 10: Block diagram of the CAFFE.

of fired wires is always referred to the superlayer multiplicity after clipping is applied. The superlayer output signals are first summed together and then split into three paths. In the first of these, the signal is discriminated to a given multiplicity level to produce the first-level DC trigger TD1 which typically requires 13 fired wires in a 250 ns window. In the second (not shown in fig. 10), the same scheme is reproduced with a lower threshold; its output is then fed into a 48-bit shift register with a 8 MHz clock for monitoring purposes. In the third the second-level DC signal, TD2, is formed according to the following scheme. First, the input signal is sampled by a flash ADC which every 62.5 ns feeds both a FIFO with programmable depth and an accumulator. At each clock the value written in the last location of the FIFO is subtracted from the value in the accumulator. After 1.2 μs the result of this operation is compared to a predefined threshold (typically corresponding to 120 hits), thus defining the TD2 signal. For monitoring purposes, the multiplicities of the superlayers are also sampled by 3-bit flash ADC's at 8 MHz.

3.3 Trigger signal generation: the TORTA board

The final first- and second-level decisions are taken by the TORTA (Trigger ORganiser and Time Analyzer) board. The TORTA performs the following functions.

- Generation of the first-level EMC trigger (TC1) using the LET multiplicities from the PASTA.
- Generation of T1 from TC1 and TD1.
- Generation of the Bhabha veto signal to inhibit T1.

- Confirmation of T1 and generation of the second level decision T2Y from TC2 or TD2.
- Vetoing of T2Y for cosmic-ray events.
- Forcing acquisition of a fraction of cosmic ray or Bhabha events, after downscaling the corresponding triggers.
- Forcing acquisition of a fraction of events with less stringent requirements, providing a minimum-bias trigger.

T1 and T2Y are distributed to the Front End Electronics (FEE) and the DAQ systems by means of the *Trigger Distributor* and *Trigger Supervisor* boards, as described below. The T1 logic has to be as fast as possible; therefore it is implemented on an ECL daughter card. The use of a small daughter card gives sufficient flexibility if a change in the T1 logic is needed. The hit configuration and the multiplicities required for generation of TC1 are loaded at the start of the run. The Bhabha trigger logic is also implemented on the TORTA. It requires the coincidence of two BBT sectors in the barrel or between the two endcaps. A given fraction of the Bhabha events is acquired for monitoring purposes. Different downscaling factors are allowed depending on the detector zone from which the BBT hits originate, as explained in section 3.1.3. These downscaling factors are loaded at run start. The trigger can be pulsed for debugging purposes either by an external signal or by an internal oscillator. Most complex functions, including the level-2 logic, dead time monitor, BBT and cosmic-ray downscaling, and readout interface, are implemented in LSI FPGA's.

3.4 Distribution of the trigger signals

The T1 signal generated by the TORTA is delivered to the *Trigger Distributor* module (TD) for synchronization with the DAΦNE radiofrequency. The resulting signal is distributed to the *Trigger Receiver* modules housed inside each calorimeter FEE crate.

The *Trigger Supervisor* (TS) provides the interface between the trigger and the data acquisition systems. Upon receipt of T1, the TS sends a T1ACK signal to the TORTA inhibiting the trigger for a programmable dead time. After a fixed delay, the TS checks for the presence of a T2Y from the TORTA to produce T2 (see fig. 11). The T2 signal is then distributed to the FIO boards which in turn drive the readout chains. There is one FIO output per FEE crate. The TS and the FIO's also manage the busy signals from the readout chains and control the synchronization cycle, which is necessary to ensure trigger number alignment in all readout modules.

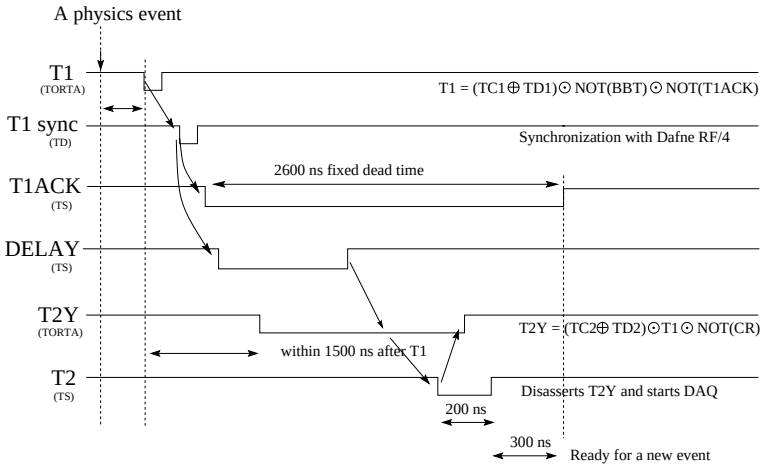

Figure 11: Normal trigger time sequence.

4 Operation of the Trigger System

KLOE has taken data in three periods, Nov-Dec 1999, July-Nov 2000, and July-Nov 2001, under very variable conditions. DAΦNE luminosity has reached $\sim 5 \times 10^{31}$ cm^{-2} s^{-1}, and background has been much higher than expected. During the 2000 run, the rate of energy deposits greater than 90 MeV on each endcap reached up to 150 kHz at the beginning of a fill. Rates in the innermost DC layers were as high as 30 kHz per wire. Threshold settings and trigger logic were therefore configured to limit the trigger rate. Vetoing Bhabha events is not necessary at low luminosity; so all Bhabhas were retained for monitoring purposes. Moreover, the large angle BBT rate was used to provide a fast measurement of the instantaneous luminosity.

Both in 2000 and 2001, trigger rates were kept at $\sim$2.5 kHz at beginning of a fill. Only about 250 Hz were due to e^+e^- collisions, Bhabha scatterings, or ϕ decays. Tagged cosmic rays acquired for calibration purposes contributed $\sim$400 Hz. About 650 Hz were due to cosmic rays escaping the veto. The remaining $\sim$1.2 kHz was from machine background, which was rejected by fast off-line filters after acquisition. Examples of various event categories are shown in fig. 12.

4.1 Operation of the EMC trigger

The EMC trigger was operated in the first-level mode. The standard trigger condition required two sectors above the LET threshold:

$$TC1 = B2M \oplus B1M \odot (W1M \oplus E1M) \oplus (E1M \odot W1M) \qquad (2)$$

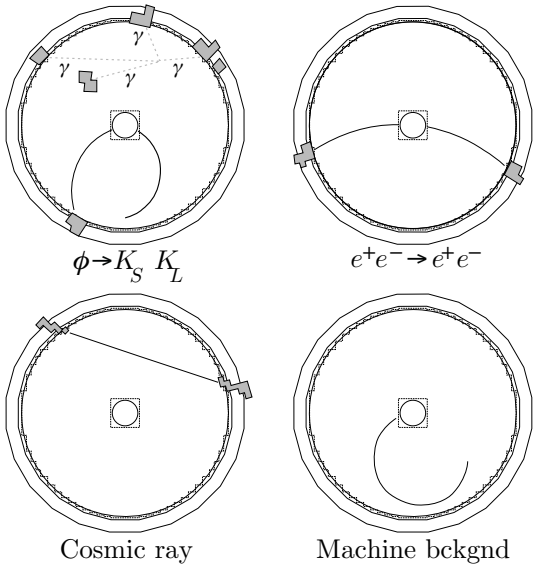

Figure 12: Example of events. The grey areas indicate energy deposits in the calorimeter.

The meaning of the above symbols is given in table 1. Typical LET threshold values were 50 MeV for the barrel sectors and 90-150 MeV for the endcap sectors. Because of

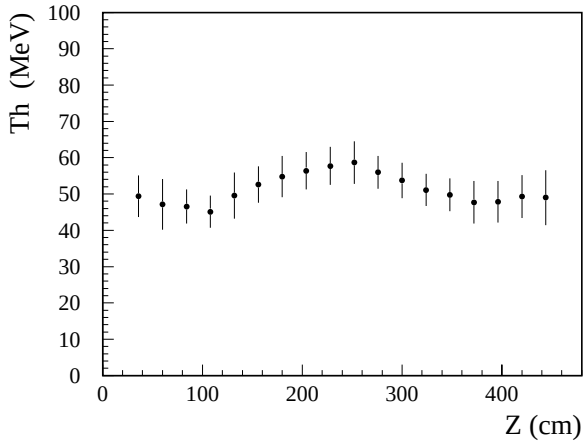

Figure 13: Threshold vs longitudinal position, z, for a barrel module.

light attenuation in the fibers, the effective threshold would vary greatly along the sector length. Use of the signal defined in eq. 1 greatly improves the uniformity of response. The threshold profile is shown in fig. 13. It is monitored run by run, comparing the trigger sector response with the energy measured by each calorimeter readout channel for various event types. The thresholds varies by less than ± 10 MeV along the module length. This variation is comparable with the EMC resolution and is negligible. The method also allows large threshold variations to be forced. Sensitivity to the high background rate

near the beam can be reduced by using a threshold dependence as shown in fig. 14 for the sectors close to the beam.

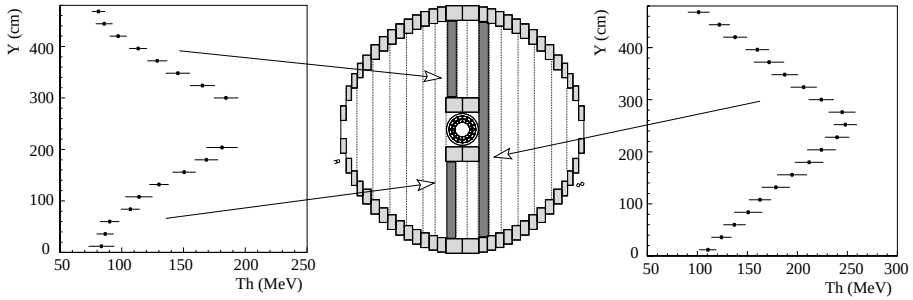

Figure 14: Thresholds close to the beam pipe are set to reduce triggering on machine background.

4.2 Operation of the DC trigger

The DC trigger was used in year 2000 with a threshold value of 13 hits for the first level, and 120 hits for the second level. With the choice of 13 hits, TD1 is on average $\sim$20 ns slower than TC1 for physics events. The DC first-level rate was 5-10 kHz at run start. The delay in TD1 increases by $\sim$5 ns for each additional hit required. The threshold for TD2 was driven by the need to reject single-track background events. Efficiency for e^+e^- collision events, for which the DC trigger is effective, remains very high. The loss of $K_S \to \pi^+\pi^-$, $K_L \to$charged events is found to be about 1 %. Fig. 15 shows the average

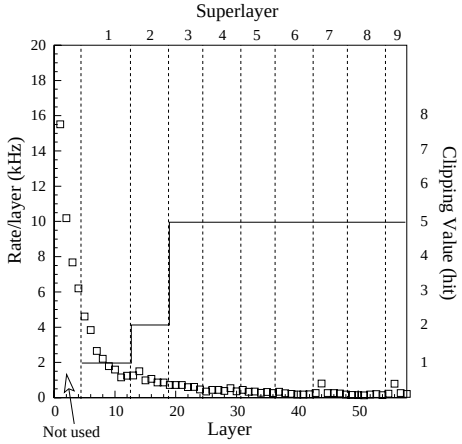

Figure 15: Average DC wire rate vs layer (open squares). Clipping values for the superlayers, are shown by the solid line.

rate per wire as a function of layer number at the beginning of a fill. Because of the large increase of rate at small radius, the first two superlayers were clipped at very low values.

Standard clipping settings are shown in fig. 15. The DC trigger rate at fill start is $\sim$1 kHz. The threshold turn-on vs number of hits is determined from full event analysis and is shown in fig. 16.

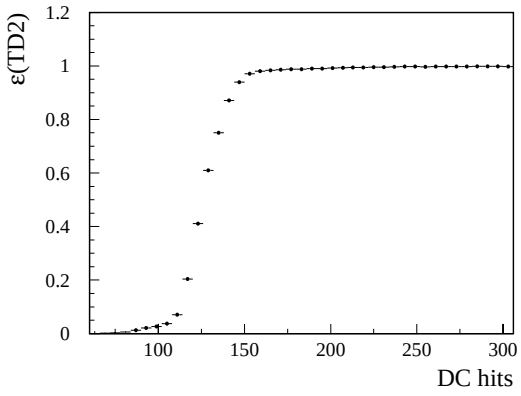

Figure 16: Threshold turn-on for the second level DC trigger.

5 Determination of trigger efficiencies

We concentrate in the following on $K_L - K_S$ events. The methods described apply to other types of events as well. A trigger emulator program has been applied to events generated by the the standard KLOE Monte Carlo. Data is however necessary for the determination of the EMC trigger efficiency for the calorimeter, since the response of the calorimeter to hadrons at very low energies is not well parameterized in available generators. The DC trigger efficiency, which is dominated by geometry, can instead be reliably estimated with the use of the Monte Carlo.

We have developed two methods to determine the trigger efficiency from data. The first method uses both the EMC and DC triggers for events with charged particles in the final state. The second method studies the EMC trigger only. Cross checks can be performed between the results of the two methods and the trigger emulator.

5.1 Method 1

Except for the case of events which give signals in the calorimeter only, we can use the fact that the DC and the EMC triggers are kept separate. Let N_{EMC}, N_{DC}, and N_{BOTH} be the observed number of events triggered by the EMC, DC, and both triggers respectively. The EMC and DC trigger probabilities, P_{EMC} and P_{DC}, are then related to the unknown

total number of produced events, N_{TOT}, through the equations:

$$\begin{aligned} N_{EMC} &= N_{TOT}\, P_{EMC} \\ N_{DC} &= N_{TOT}\, P_{DC} \\ N_{BOTH} &= N_{TOT}\, P_{EMC} P_{DC}\, C_T \end{aligned} \tag{3}$$

where C_T accounts for possible correlation between the two triggers. For totally uncorrelated triggers (C_T = 1) $P_{EMC} = N_{BOTH}/N_{DC}$ and $P_{DC} = N_{BOTH}/N_{EMC}$. Use of Monte Carlo simulation is necessary to estimate C_T, which turns out to be $\sim$1.01 for all relevant decay channels. The correlation between the triggers can also be examined using data. Fig. 17 shows the dependence of the variable N_{BOTH}/N_{DC} on the TD2 threshold for $K_L \to \pi^{\pm} e^{\mp} \nu_e$ and $K_L \to \pi^{\pm} \mu^{\mp} \nu_\mu$ decays. For threshold values around the nominal

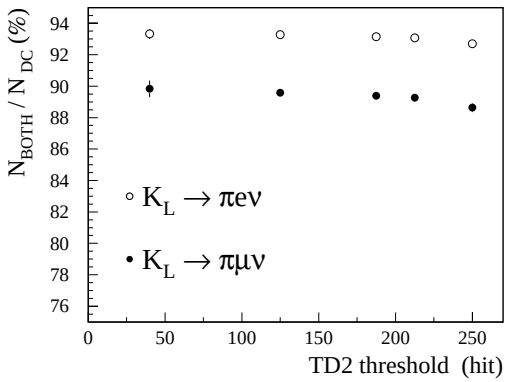

Figure 17: Distribution of N_{BOTH}/N_{DC} for K_L semileptonic decays vs number of hits.

setting of 120, it is constant to within 1% for both samples, in agreement with Monte Carlo expectations. Results for P_{DC} and P_{EMC} are listed in the first and second column of table 2.

5.2 Method 2

This estimate relies on separating the EMC clusters due to K_S and K_L decays. One can thus determine the unbiased probability for a K_S (K_L) to fire 0,1,2... sectors using events in which the K_L (K_S) has satisfied the trigger conditions alone. Combining these probabilities, the efficiency for all types of decays is given by:

$$\epsilon_{trig} = 1 - [S(0)L(0) + S(1)L(0) + S(0)L(1)] \tag{4}$$

where $S(i)(L(i))$ is the probability for a K_S (K_L) to fire i trigger sectors of the calorimeter. We need to choose the events which allow the best separation of K_L and K_S clusters. For K_S decays, this is given by events where the K_L reaches and interacts in the

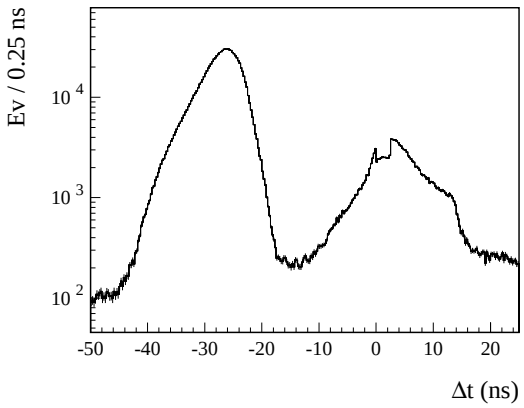

Figure 18: Time difference between K-crash and all other clusters, for $K_S \to \pi^0\pi^0$ decays.

calorimeter (K-crash), because of the excellent calorimeter time resolution and the fact that $\beta(K_L) \sim 0.213$ [7]. Fig. 18 shows the distribution of the time difference between the K-crash cluster and all other clusters for $K_S \to \pi^0\pi^0$ events. The early peak corresponds to photons from π^0 decay. Late times are from the K_L. A cut at -15 ns cleanly separate the two samples. The same method is used for $K_S \to \pi^+\pi^-$ events. For K_L decays in flight, we select events with four photons from $K_S \to \pi^0\pi^0$ decay. The remaining clusters are assigned to the K_L. Finally, for each category of events, the probabilities that the K_S and the K_L generate a trigger (estimated using K-crash and $K_S \to \pi^0\pi^0$ events respectively) are combined according to equation 4, to obtain the trigger efficiencies in table 2.

5.3 Results

Table 2 gives the results of our efficiency studies for the 2000 data. The drift chamber trigger is highly efficient for those events for which the calorimeter trigger probability is lower. The overall trigger efficiency is close to unity for all decay channels.

For events with a reconstructed K_L decay (first four raws of the table), the uncertainty is determined by the statistics of the samples used and by the assumption that the simulation reproduces the correlation between the two triggers to within 10%. The agreement between the calorimeter efficiencies from the two methods is better than 1%.

For $K_S \to \pi^+\pi^-$, K_L crash events, the correlation between the two triggers cannot be reliably estimated by Monte Carlo and is not taken into account.

Decay Channel	DC (1) Eff., %	EMC (1) Eff., %	EMC (2) Eff., %	Overall Eff., %
$K_S \to \pi^+\pi^-$, $K_L \to \pi^+\pi^-\pi^0$	98.8 ± 0.1	96.0 ± 0.1	95.7 ± 0.4	99.4 ± 0.1
$K_S \to \pi^+\pi^-$, $K_L \to \pi^\pm e^\mp \nu_e$	98.4 ± 0.1	93.2 ± 0.1	93.3 ± 0.3	98.9 ± 0.1
$K_S \to \pi^+\pi^-$, $K_L \to \pi^\pm \mu^\mp \nu_\mu$	98.2 ± 0.1	90.0 ± 0.1	90.1 ± 0.4	98.7 ± 0.1
$K_S \to \pi^+\pi^-$, $K_L \to \pi^0\pi^0\pi^0$	83.2 ± 0.2	99.8 ± 0.1	99.7 ± 0.1	99.9 ± 0.1
$K_S \to \pi^0\pi^0$, K_L crash	-	-	99.86 ± 0.04	99.86 ± 0.04
$K_S \to \pi^+\pi^-$, K_L crash	83.2 ± 0.1	99.53 ± 0.02	98.3 ± 0.2	99.8 ± 0.1

Table 2: Trigger efficiencies computed from data using the two methods described.

5.4 Acknowledgments

We want to deeply thank our institutes' technicians. In particular:

A. Balla and G. Corradi for their fundamental contribution in the design, construction and installation of the calorimetric trigger.

M. Gatta for the design and construction of several parts of the drift chamber trigger.

M. Carletti, G. Paoluzzi, G. Papalino and M. Santoni for their support in the installation of the entire system.

We want to acknowledge the support of the Electronic Service of the Sezione INFN of Bari, in particular of R. Liuzzi and C. Pinto.

We also want to thank F. Bertino and D. Riondino of the LNF Electronic Service.

Work partially supported by German Ministry of Education and Research (BMBF) under contracts (06 KA 654 TP3), (06 KA 564 TP2), (06 KA 860), (06 KA 957)

Work partially supported by Graduiertenkolleg 'Elementarteilchenphysik an Beschleunigern', Deutsche Forschungsgemeinschaft

Work partially supported by EURODAPHNE network, contract No. FMRX-CT98-0169

Work partially supported by INTAS contracts No. (96-624) and (99-37)

Work partially supported by TARI contract HPRI-CT-1999-00088

References

[1] The KLOE Collaboration, *KLOE: A General Purpose Detector for DAΦNE*, LNF-92/019(IR) (1992).

[2] The KLOE Collaboration, *The KLOE Detector, Technical Proposal*, LNF-93/002(IR) (1993).

[3] The KLOE Collaboration, *The tracking detector of the KLOE experiment*, Nucl. Inst. Meth. A (2001), in press.

[4] The KLOE Collaboration, *The KLOE electromagnetic calorimeter*, Nucl. Inst. Meth. A 482, 363-385 (2002).

[5] The KLOE Collaboration, *The KLOE Data Acquisition System, Addendum to the Technical Proposal*, LNF-95/014 (1995).

[6] The KLOE Collaboration, *The KLOE Trigger System, Addendum to the Technical Proposal*, and references therein, LNF-96/043 (1996).

[7] The KLOE Collaboration, *Measurement of the branching ratio of the decay* $K_S \to \pi e \nu$, LNF-02/001 (P).